Infrared analysis and pressure measurements on a single loop pulsating heat pipe at different gravity levels

D. Mangini[1], M. Pozzoni[2], M. Mameli[3], L. Pietrasanta[1], M. Bernagozzi[1], D. Fioriti[3], N. Miché[1], L. Araneo[4], S. Filippeschi[3], M. Marengo[1].

[1]*School of Computing, Engineering and Mathematics, University of Brighton, Lewes Road, BN2 4GJ Brighton, UK*
[2]*University of Bergamo, Via Galvani, 2, 24044 Dalmine BG, Italy*
[3]*DESTEC, University of Pisa, Largo Lucio Lazzarino 2, 56122 Pisa, Italy*
[4]*Polytechnic of Milan, Via Lambruschini 4A, Milan, Italy*

Abstract

A Single Loop Pulsating Heat Pipe (SLPHP) with an inner diameter of 2 mm is tested in hyper/micro gravity conditions during the 68th ESA Parabolic Flight Campaign. The system is designed with two sapphire tubes that connect the heated and the cooled section, allowing simultaneous fluid flow high-speed visualization, and a direct to fluid IR analysis by using respectively a high-speed camera and a Medium-Wave Infrared Camera (MWIR). Three independent heaters are positioned at the evaporator in order to vary the power distribution and to promote different flow motions with specific heating configurations. Furthermore, two highly accurate pressure transducers measure the pressure drop between the condenser and the evaporator. Additionally, twelve thermocouples mounted on the external tube wall record local temperatures during parabolic flight tests. Such a complete thermo-fluid dynamic analysis at different gravity levels, coupled with the acquisition of high-speed and infrared images in the transparent section of the SLPHP, has the main objective of providing a better understanding on the relationship between the fluid flow motion and the thermal response of the device. Infrared Time-space temperature maps of the flow are correlated with pressure measurements, the external wall tube temperatures, the liquid slug velocity and the local void fraction; providing an exhaustive overview of such a PHP transparent tube both in microgravity and hyper-gravity conditions. Additionally, for the first time in microgravity, the effect of the condenser temperature on PHPs is explored. When the condenser temperature is set at a higher value than the environment, results highlight that the possibility to invert the flow motion direction by means of non-symmetrical heating configurations is hindered. These experimental data could assist the development of improved numerical models of Pulsating Heat Pipes at different gravity levels.

Keywords: Pulsating Heat Pipe; Infrared analysis; Microgravity experiments.

1. INTRODUCTION

The constant demand for innovation in heat transfer solutions, for compact and more powerful electronics, is driving the research towards new technologies able to dissipate more power in less space and with high reliability standards. The Pulsating Heat Pipe (PHP) is relatively recent in the heat pipe family, even if the first patent dates back to almost 30 years ago [1]. Due to their build simplicity, the ability to dissipate heat also in microgravity and their compactness, PHPs could represent an alternative to cooling systems in the near future, both for ground and space applications. Nevertheless, the interest of the scientific community is still focused on this technology due to its phenomenological complexity [2]. PHPs have not reached a full industrialization phase yet, because of unsolved issues affecting PHPs performances [3] (evaporator dry-out, geometrical design best practice, fluid selection and flow pattern transition prediction, for instance) that result in a lack of a tool able to guide engineers during the design phase. Efforts have to be made to explain and to model the highly-coupled thermo-hydrodynamics of PHPs [4]. Regarding space applications, where it has been proven that PHPs can operate, a reduction in performance is experienced [5][6] and the role of inertial forces and surface tension on obtaining a stable functioning state has still to be understood. Hence, it raises the aim to support the PHPs development from functional verification in laboratory environment (TRL4, according to European Space Agency, ISO 16290:2013) to a critical function verification in relevant environment (TRL5) through a long-term microgravity investigation onboard the International Space Station. Given the complexity of the thermofluidics phenomena occurring inside a PHP, experimental research has also been driven to analyse single phenomena, while preserving the operational regimes of the PHPs [7]. In such perspective, a full thermo-fluid characterization of a Single Loop PHP (SLPHP), which can be considered the basic constituent of a more complex multi-turn Pulsating Heat Pipes, is fundamental for the complete description of the working principles. Additionally, even if it is already demonstrated that

a certain number of U-turns is necessary to make the overall PHP performance almost independent of gravity [8], a complete characterization of a PHP with a simplified geometry both in microgravity and in hyper-gravity can decrease significantly the computational costs for the validation of lumped parameter models [9][10] and novel CFD simulations [11][12]. Furthermore, such a geometric simplification allows a detailed study on the local scale of single physical aspects, rather than focusing on the overall performances. Vapour temperature and quality [13], role and thickness of the liquid film surrounding vapour plugs [14], wetting and de-wetting phenomena of a moving liquid slug [15], effect of dominant flow patterns and flow pattern transition [16], are some of the open questions to be tackled over a wide range of operating conditions. A review of the last 10 years cutting edge techniques applicable for the investigation of local phenomena in PHPs is summarised in Table 1. There is a compelling necessity of direct non-intrusive measurements on the fluid that do not affect the fluid-dynamics, thus, Infrared (IR) techniques are getting the attention of research groups, especially using an IR transparent medium (germanium or sapphire inserts) that allows the direct fluid temperature measurement. The aim of this work is to study the effect of changing gravity level on the local phenomena of flow pattern transition, wetting/dewetting of the internal tube wall during the oscillating /pulsating motion, correlating such fluid-dynamics aspect with pressure measurements of the flow. A high-speed Mid-Wave Infrared (MWIR) is used to measure the liquid bulk temperature at different gravity levels, thanks to two sapphire inserts on the adiabatic region of the SLPHP [17]. The loop is also equipped with high-accuracy pressure transducers in evaporator and condenser areas and with high-speed visible imaging. This set-up has been implemented on a rack with an auxiliary cooling system to accurately control the condenser temperature.

Table 1. Evolution and aims of innovative techniques of investigation in milli/micro fluidic systems

Author, Year	**Measurement technique**	**Geometry**	**Flow type**	**Channel cross-section**	**Fluid**	**g level**	**Aim of the investigation**	**Investigated area**
Luciani et al.[18], 2009	Indirect TC	Single Channel	Flow Boiling	Rectangular, Hy-Diam.: 0.49, 0.84, and 1.18 mm	HFE-7100	PF	Inverse Heat Conduction Problem	Evaporator
Hetsroni et al.[19], 2011	Direct IR	Multi-channels	Laminar single phase	Rectangular, 320x750 um	Water	1g	Fluid temperature	Heated
Mehta and Khandekar [20], 2012	Indirect IR	Single channel	Laminar single phase	Square 5mm	Water	1g	Heat flux	Heated
Gully et al. [13], 2013	Direct micro-TC	Single channel	Pulsating	Stain-less steel tube, I.D/O.D=2mm/3mm	Liquid oxygen	1g	Vapour temperature	Evaporator
Karthikeyan et al. [21], 2014	Indirect IR	CLPHP	Pulsating	Copper tube, I.D/O.D=2mm/3mm	Water	1g	Flow regimes	Evaporator, Adiabatic
Chauris et al. [22], 2015	Indirect IR	Single channel	Flow boiling	Copper tube, I.D/O.D=2mm/2.4mm	Water	1g	Film Heat transfer	Adiabatic
Spinato et al. [23], 2015	Time-strip image processing	SLPHP	Pulsating	Square 1x1mm	R245fa	1g	Flow regimes, Interface dynamics	Evaporator, Condenser
Liu and Pan [24], 2016	Direct IR	Single channel	Flow boiling	Germanium\Aluminium, rectangular 250umx1mm	Ethanol	1g	Fluid temperature, Flow regimes	Evaporator
Fourgeaud et al. [25], 2017	Grid deflection, Interferometry	Single channel	Pulsating	Rectangular, 2x22mm^2	Ethanol	1g	Film Dynamic	Evaporator

2. EXPERIMENTAL APPARATUS

In Fig. 1 the experimental apparatus of the SLPHP test cell is shown. It consists of an evaporator and a condenser made by two copper pipes to minimize the thermal resistances (I.D. /O.D. 2mm/4mm, 120mm axial length), and an adiabatic zone made by two sapphire tubes (I.D./O.D. 2mm/4mm,

110mm axial length) with average transmission coefficient 90% in the medium infrared spectrum (*3 ÷ 5 μm*). The device is partially filled with FC-72 with a volumetric ratio of 0.6, which corresponds to 1.45 ml of liquid. The adiabatic section is connected to the evaporator and the condenser via four brass joints sealed with vacuum epoxy (Henkel Loctite® 9492). As shown in Fig. 1, on the right branch of the SLPHP, two high-accuracy pressure transducers (Keller® PA(A)33X, 1 barA, Accuracy 50 Pa) are hosted in the brass junctions at the ends of the sapphire tube. The sapphire sections allow thermographic analysis by means of a high-speed and high-resolution MWIR camera (AIM® from TEC-MMG owned by ESA/ESTEC), whose main specifications are listed in Table 2.

Table 2. MWIR Camera specifications.

Spatial resolution	1280x1024
Temporal resolution	50 fps in full frame
Bandwidth	3-5 μm
Transmission	≈93%
Maximum resolution	40 μm
Sensor temperature	60 K
Thermal Resolution	±0.05K

The visualization equipment is completed by a compact high-speed camera (Ximea® USB3 XiQ-093) and by a mirror system that allows the simultaneous observations of both sapphire tubes.

On the left branch of the SLPHP there is a micro-metering evacuating\filling valve (Microcolumn®, UP447) hosted in the bottom brass junction, guarantying a leak rate down to 10^{-8} mbarl/s. The evacuating\filling procedure is the following: the device is firstly vacuumed down to 0.3 mPa with an ultra-high vacuum system (Varian® DS42 and TV81-T) and then partially filled up with pure FC-72, previously degassed to extract non-condensable gases, following the procedure indicated by Henry et al. [26]. The evaporator is equipped with three independently controlled heating wires (Thermocoax®, Single core 1Nc Ac), providing a wall to fluid heat flux of 7.64 W/cm^2 at 12 W. As illustrated at the bottom of Fig. 1, two heaters (Heater L and Heater R) are placed just above the turns of the evaporator and the remaining (Heater C) is placed in the horizontal section. This configuration provides a non-uniform heating pattern that, as previously demonstrated by Mameli et al. on ground for a similar device [27] , allows the establishing of a circulation of the working fluid in a preferential direction, which improves the overall thermal performance of the device [18]. Heat is dissipated in the condenser section by means of a shell and tube heat exchanger. The heat exchanger is connected to an external water cooling loop that controls the liquid temperature via a Peltier array of 10 elements (European Thermodynamics® ETC-288-10-05-E). The cooling loop also provides fixed temperature water to a black-painted aluminium plate placed behind the right branch of the SLPHP, which serves as a high-emissivity, constant low temperature background to increase the temperature range in the IR imaging, allowing a more detailed detection of the features of the liquid in the sapphire.

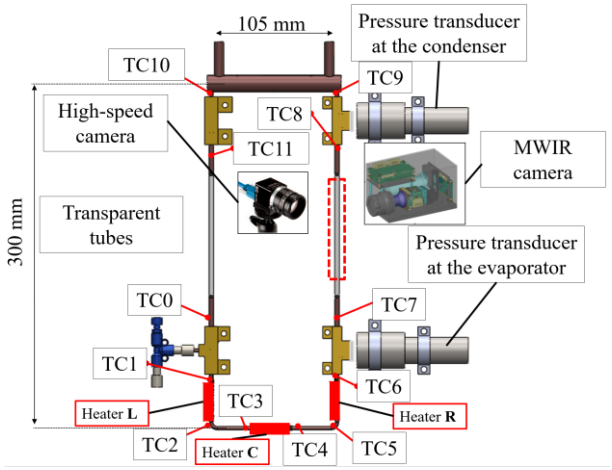

Fig. 1. SLPHP apparatus with visualization and pressure acquisitions schematic, thermocouples and heating elements position in red.

This makes it possible to also appreciate the liquid film dynamics during experiments, as already suggested by Mangini et al. [28]. Temperature, pressure and g-level data are record and monitored by means of an acquisition system, composed by: NI cRIO 9074® and NI 9205®, NI 9264®, NI 9871® modules. A custom LabVIEW® software provides a synoptic control panel for a real time monitoring and independent control of power input at the three heaters. The temperature and pressure measurements are synchronized with the images recorded by the high-speed camera (60s at 200 fps each acquisition) and the IR images (20s at 50 fps each acquisition).

3. EXPERIMENTAL PROCEDURE

This experimental campaign intends to analyse the thermo-fluid dynamics behaviour of the SLPHP through pressure and temperatures measurements, together with high-speed and infrared visualizations at different gravity levels, with particular attention to:

- Highlighting the relation between pressure and temperature measurements and the flow patterns, deducing time-space maps of the fluid

temperatures measured by the IR camera and correlating them with the liquid slug velocity, the void fraction, the pressure measurements and the external wall tube temperatures at different gravity levels.

- Understanding the liquid film dynamics with the proposed IR technique, both in micro and hyper-gravity conditions.
- Understanding the effects of the condenser temperature on the overall behaviour of the device.

The set-up was tested during the 68th ESA PFC, which scheduled over three days 93 parabolae and where every parabola gives roughly 20 seconds of microgravity. Moreover, the parabolae are divided in sets of five, alternated by five minutes breaks and one longer 15min break between the 15th and 16th parabola. The SLPHP is tested in Bottom Heated Mode, with the evaporator section below the condenser. The condenser temperature is varied between 15°C, 30°C, 7°C during Day 1, Day 2, Day 3, respectively, and kept constant throughout the whole flight.

Table 3. 68th ESA PFC experimental matrix.

Config. name		Heater Power Input [W]			Condenser temperature [C]		
		Left	Centre	Right	Day I	Day II	Day III
Clockwise	A	6	3	0	15	30	7
	B	6	6	0			
	C	9	6	0			
	D	12	9	0			
Anti-clockwise	E	0	3	6			
	F	0	6	6			
	G	0	6	9			
	H	0	9	12			

The heat power inputs are varied at every set of five parabolae both in intensity and in distribution over the three heaters, as summarised in Table 3. The power at the evaporator ranges from a minimum of 9 W to a maximum of 21 W.

4. RESULTS AND DISCUSSION

With the previously described layout, the IR camera is focused on the sapphire insert between the two pressure transducers. IR acquisition is performed either during microgravity periods, or during the transition between hyper-gravity and microgravity. In Fig. 2b the qualitative benefit of the IR imaging compared to the visible imaging can be appreciated, highlighting the liquid film evolution along the channel. In case of annular or semi-annular flow, the IR analysis can be considered a useful tool to appreciate the liquid film dynamics during the PHP operation at different gravity levels. The IR camera detects higher temperatures where the liquid film thickness is higher, since the emissivity is directly proportional to the liquid film thickness. This allows to track the motion of capillary ridges along the sapphire insert, where just a slight contraction of the vapour bubbles can be visible from the high-speed camera (point A in Fig. 2b).

Fig. 2a shows the synchronization of both high-speed and IR imaging with the gravity variation and the measurements of pressure and evaporator temperature during 20 seconds where the transition between hyper and microgravity happens.

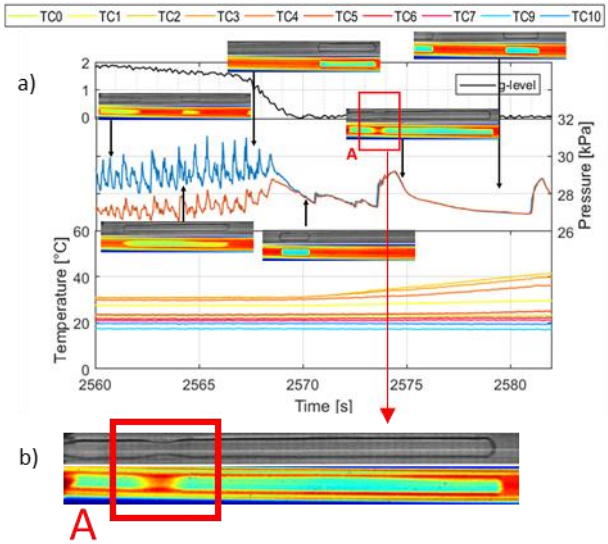

Fig. 2. a) Synchronized high-speed and IR visualization with gravity levels, pressure and temperature during transition between hyper- and microgravity (Parabola 7, Day 1). b) Zoom of one IR image and the synchronized one obtained with the high-speed camera.

The effect of the varying gravity is clearly visible on the pressure and the evaporator temperature signals. When the device is gravity-assisted, a preferential direction of the flow motion occurs, thanks to the non-symmetrical heating distribution provided at the evaporator, as already pointed out in several works [17,28]. In the heated branch, the liquid batches are pushed from the evaporator to the condenser by the expanding vapour bubbles. The gravity head assists the return of the condensed fluid from the cooled zone down to the evaporator. The coupled effect of expanding vapour bubbles in the heated branch and the gravity head in the adjacent one is the main reason of the two-phase flow circulation within the loop in hyper- and standard-gravity. The circulating flow improves also the overall heat exchange, stabilizing the temperatures at the evaporator (first half of Fig. 2a, related to

hyper-gravity). From the visualization, an annular flow is observable in the up-header, and a slug/plug flow in the down-comer. This is due to the local high heat flux provided just below the up-header that generates a vapour column continuously flowing from the evaporator to the condenser.

A clockwise motion is established during the first set of parabolae (Configuration A, B, C, D in Table 3). Since the heating element A is switched on and the heater B is off for all this set of configurations, the flow is pushed from the evaporator to the condenser from the left side of the device (looking at the front), while it returns through the right hand side branch helped by gravity. Then, the heating power is switched off during the 15min pause to allow the return of the evaporator temperatures at the environmental conditions. Approximately 3min before parabola 16, the heating power is again on at the evaporator to stimulate an anti-clockwise motion (Configuration E, F, G, H in Table 2). Indeed, for all of these heating configurations, this time the heater just below the left branch dissipates power, while the heater A is off. Therefore, an anti-clockwise motion was easily achieved during tests performed imposing a condenser temperature of 15˚C during tests performed with such configurations (Day I).

On the contrary, under the same heating configurations and with the same thermal history, the inversion of the flow was not achieved during the Day II (Table 3), when the condenser temperature was set at 30 ˚C. The device reaches a thermal crisis, as all the temperatures close to the evaporator increase abruptly, reaching 80˚C during the set of parabolae from 16 to 20 (Fig.4). Therefore, the heating power was disabled, to prevent damages at the transducers. Having the condenser at a temperature higher than the environment, the local pressure at the condenser is higher than that one at the bottom. It can be speculated that such an overpressure hinders the stabilization of the anti-clockwise flow. Setting the condenser temperature at 7˚C during Day III (Table 3), the fluid starts to oscillate without any heating power. The temperature difference between the bottom (close to the environment temperature at 18˚C) and the top (kept constant at 7 ˚C by the Peltier system) of the device is already enough to sustain a flow oscillation also without providing power. In this case, the device is heated up by the environment by means of natural convection, establishing a self-sustained flow motion. Switching off the heaters after parabola 15, the flow continues to circulate in a clock wise direction. After the 15min pause between parabola 15 and 16, the attempt to establish an anti-clockwise motion within the loop in 1-g providing the configuration “E” is hindered by the inertial effects that tend to maintain the fluid flow in the opposite direction.

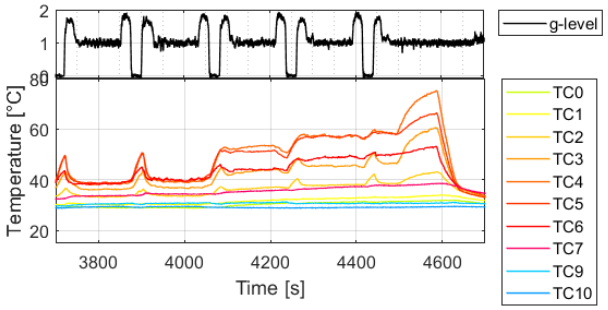

Fig. 3. Evaporator temperatures from Parabola 16 to 20, Day 2

The flow inversion is only achieved in hyper-gravity, where the higher gravitational assistance allows to gain the opposite inertial effect, establishing an anti-clock wise motion that is going to be maintained, as shown in Fig. 4a for parabola 16.

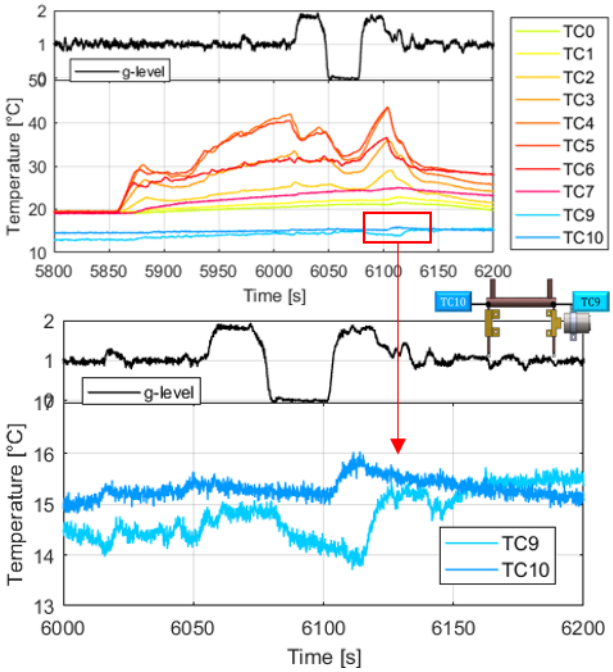

Fig. 4. Evaporator temperatures and gravity variation during Parabola 16 of Day III (a) with a highlight on TC9 and TC10 (b) to describe the inversion of the fluid motion direction after hyper-gravity.

Fig. 4b presents the temperature measurements at the two ends of the condenser. Initially, the right side of the condenser zone has a higher temperature (recorded by TC10) than that one recorded by TC9 (positioned in the left side). Indeed, since at the beginning the flow is circulating clock-wise, the flow with a higher temperature pushed by evaporation phenomena at the evaporator is coming from the right side of the device, and then returns

refreshed from the left one. The occurrence of the anti-clockwise motion is achieved only during the second hyper-gravity period. Indeed, after such an increase of the gravity level, the temperature recorded by TC9 starts to be higher than TC10.

These preliminary results related to the condenser temperature effect at different gravity levels in a simplified PHP point out the importance of this parameter on the overall thermo-fluid dynamics, suggesting a further deeper investigation in a wider condenser temperature ranges. This is particularly relevant for possible future space applications, where the heat-rejecting area temperature is usually not controlled and variable.

During the microgravity phase the definition of the "down-comer" is not valid anymore, in the sense that there isn't any more a gravity head able to push down the flow through the non-heated branch of the loop. The thermo-fluid dynamic behaviour in weightlessness is damped and intermittent. The pressure exhibits only isolated peaks, interspersed by a flat trend, synonymous of prolonged overall flow stop-overs. Being a PHP with just one loop, a self-sustained flow cannot be achieved without gravity assistance. The temperature evolution of the liquid slugs during stop-overs in microgravity can be appreciated in Fig. 5a, where consecutive IR frames of the sapphire tube are paired with the pressure measurements in a 180ms interval during 0.15 s of the microgravity period of parabola 2 of Day 1. The lack of fluid motion is confirmed also by the flat trend of the pressure, together with the shape of the vapour bubbles' contact angles. There is no visible curvature difference in the slug menisci, as shown in Fig. 5b. Moreover, temperature gradients can be easily detected by the IR measurements, thanks to the high sensitivity of the IR camera (0.05 K). A temperature gradient of approximately 2˚C is measured between the three liquid slugs that are detected along the sapphire insert, as presented in Fig. 5a. During stop-overs, heat is mainly exchanged by conduction between the wall and the stagnant fluid and liquid slugs close to the evaporator are heated up by the power dissipated by the heating elements, resulting in a local increase of the liquid bulk temperature.

During the sporadic peaks of pressure in microgravity, a direct comparison between the pressure measurements and the IR images can be established (Fig. 6). In the first half of the frames of Fig. 6a, the bubble motion from the evaporator to the condenser is vigorous (push), then it decelerates, starts to undergo in the opposite way (inversion) and finally stops after an even quicker impulse toward the condenser (stop).

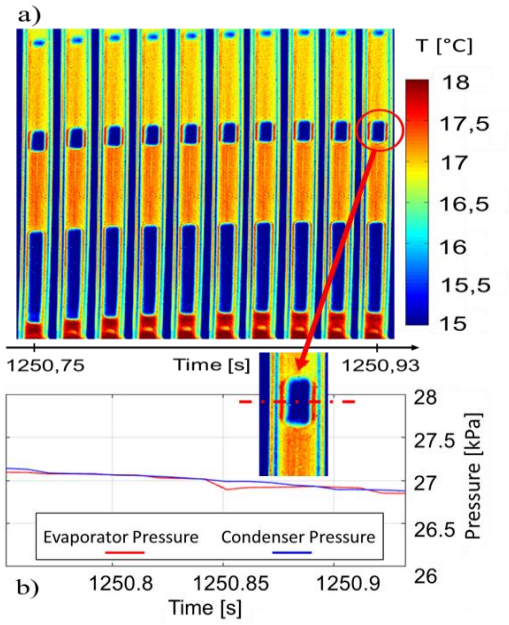

Fig. 5. Absence of motion during microgravity: a) IR frames (50 Hz); b) pressure, g-level and single bubble zoom.

All these motions are identified in the graph of Fig. 6b, overlapping the evaporator and the condenser pressure. In the last frames the fluid stops, and therefore the two signals show a flat trend. It can be noticed that the temperatures recorded by the IR camera in the presence of vapour bubbles during such oscillations are higher than the backscreen temperature. This is due to the liquid film deposited on the inner wall tube surface. A certain amount of liquid is entrained and deposited on the inner surface during liquid plugs oscillations. This wetting phenomenon is appreciable by means of the proposed IR analysis. An annular flow is detected when boiling processes produce a vapour column in the sapphire insert. In case of annular flow, the information given by the IR is only partial, since the emissivity ε of the fluid is dependent by its thickness [29]. At this stage, in case of annular or semi-annular flow, the IR visualization can be a useful tool to qualitatively appreciate the liquid film dynamics during the PHP operation in microgravity (Fig. 7). In Fig. 7a, the deposition of the liquid film on the internal wall of the sapphire tube during microgravity period is particularly evident from the yellow colour surrounding the bubbles. Moreover, the dynamic of capillary ridges can be appreciated from the IR images between the elongated bubbles. When the liquid film becomes locally thicker it can form a liquid meniscus enclosing completely a bubble (highlighted by the black circle in Fig. 7a).

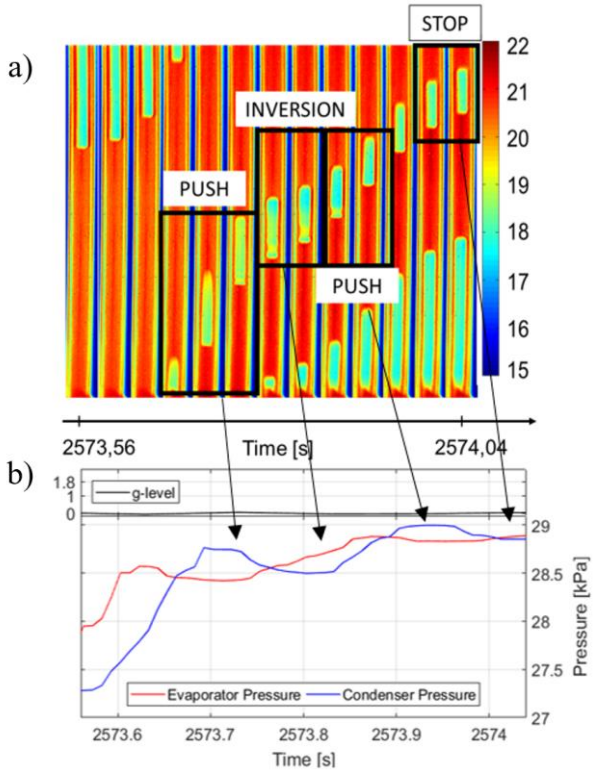

Fig. 6. Pressure peaks during microgravity: a) IR frames (16.6 Hz); b) pressure and g-level.

This meniscus acts as a barrier to the stream of vapour and restores the slug/plug flow, hence consequently leads to the expansion of the abovementioned bubble.

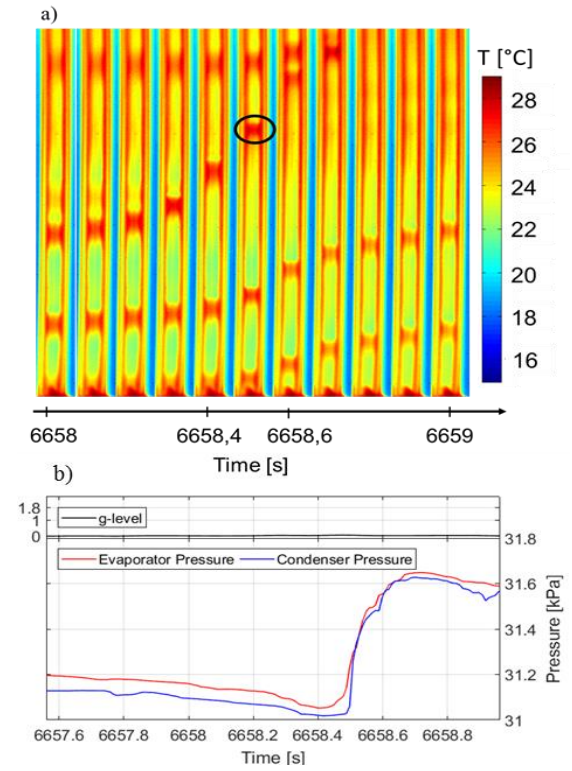

Fig. 7. Semi-annular flow during microgravity: a) IR frames (10Hz); b) pressure and g-level.

The expansion pushes the two-phase flow towards the condenser, causing a sudden peak of the pressure (Fig. 7).

In Fig. 8 a 180ms interval during the hyper-gravity period of parabola 2 of Day 1 is presented. It is possible to appreciate the increased pressure gradient between evaporator and condenser compared to the microgravity cases, due to the gravitational component and the inertial component to the overall ΔP in the channel.

As highlighted by the zoom of Fig. 8b, both the leading edge and the trailing edge of the bubble are recognizable in the first frames, when the bubble moves, whereas over the last frames they are not distinguishable anymore, as the bubble stops. The liquid plug motion, that drags and subsequently deposits upon the inner tube wall surface a certain amount of the liquid film is appreciable from the IR images close to the front menisci of the vapour bubbles.

Furthermore, with respect to the microgravity case, Fig. 8a displays a reduced temperature gradient between the two ends of the sapphire tube.

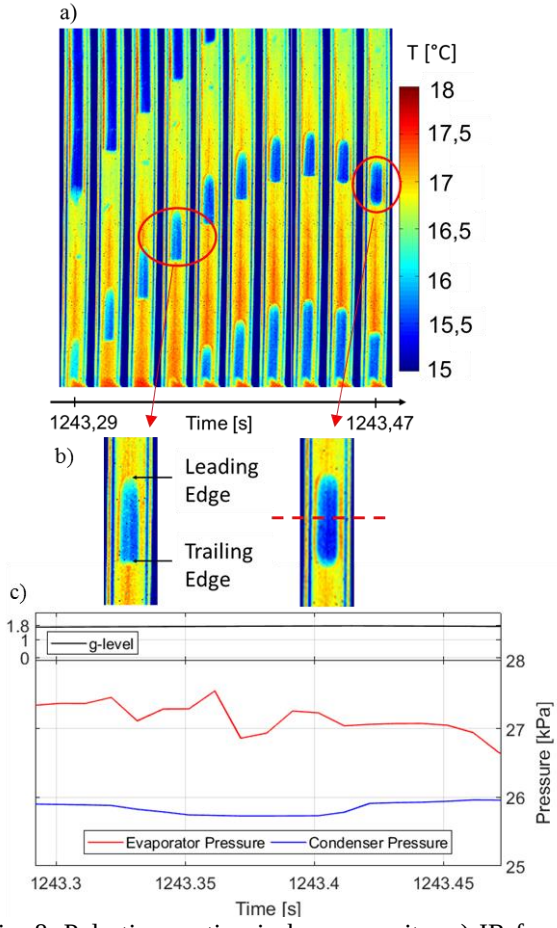

Fig. 8. Pulsating motion in hyper-gravity: a) IR frames (10 Hz); b) single bubbles zoom; c) pressure and g-level.

Since the flow motion continuously dissipates efficiently heat, decreasing the difference of temperature between the heated and the cooled region, the liquid slugs along the sapphire insert also have a lower temperature gradient than the one measured in the stop-over case (Fig.5).

Additionally, the averaged slug-plug flow velocity (V_{avg} in Fig. 10d), together with the void fraction (α, in Fig. 10c) are estimated using the high-speed images obtained in the transparent sections at 200 fps. The velocity of the liquid phase has been evaluated via a multiple-position, liquid phase sensitive, PIV-based velocimetry method [30]. The void fraction has been obtained via a binarization of the images and the volume evaluated as a sum of the infinitesimal cylinders with as diameter the number of pixels with logic value 1 in each columns of a vapour plug (d_{i-th}) and as height 1 pixel, as described in Fig. 9.

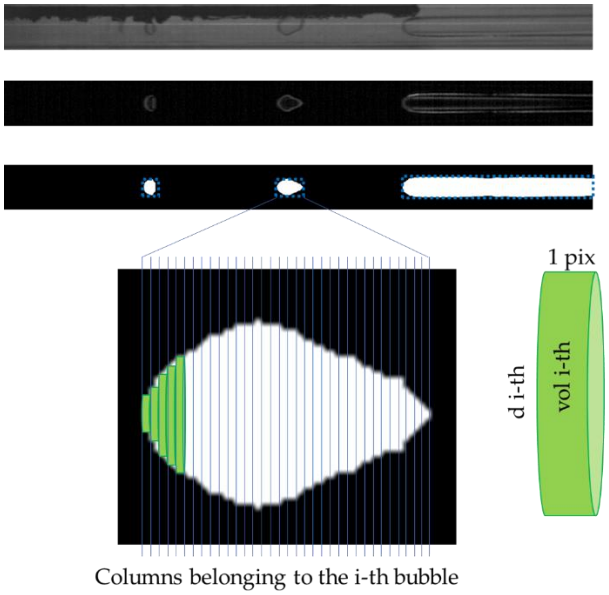

Fig. 9 Binarization process and vapour volumes evaluation as a sum of infinitesimal cylinders

By means of the thermographic analysis it was also possible to obtain a time-space map of the temperature evolution along the sapphire tube both in micro and hyper-gravity conditions. Fig. 10e presents the spatial and temporal temperature evolution on 10 mm of the vertical central axis in the middle of the sapphire tube. On the y-axis are reported the values of the temperature for 10 mm along the sapphire pipe, while on the x-axis the different time instants where the temperature is evaluated. They are combined with the gravity level variation and the temperatures recorded by the thermocouples TC7 and TC8, which are at the two ends of the sapphire tube respectively. The estimated maximum error on the IR temperature measurements is ±1.5K, in accordance with the lumped parameter model obtained by Catarsi et al. [31]. V_{avg} and α are correlated with the time-space temperature map and the difference of pressure measured at the edges of the sapphire insert in weightlessness.

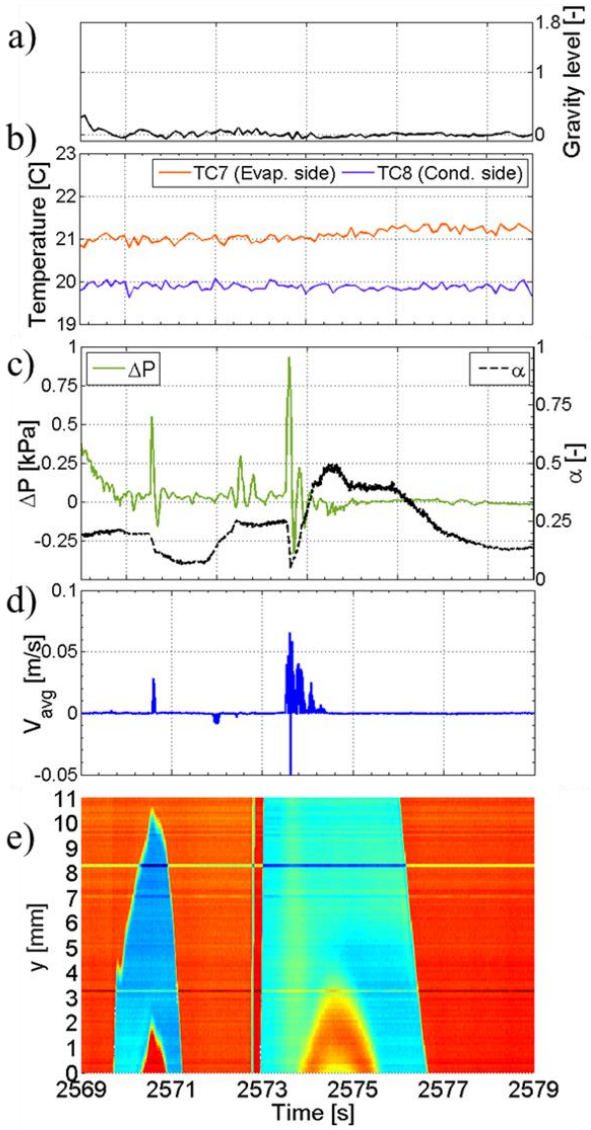

Fig. 10. a) Gravity level, b) External tube temperatures at the edges of the sapphire, c) Pressure difference, d)Liquid velocity and void fraction and e)time-space temperature map of the fluid synchronized during microgravity oscillations.

From Fig. 10, the continuous alternation of stop-over periods and sporadic oscillations in microgravity can be easily recognised by the measured pressure variation, the slug/plug flow velocity and the α trend. During stop-overs, the pressure difference is negligible, and no significant variations of the two-phase temperatures are detected. During flow oscillations, the pressure difference can reach 1 kPa, while the slug/plug flow

velocity can reach up to 5 cm/s in microgravity for this configuration. The time-space map of the 10 mm of the axial length of sapphire tube analysed during such oscillations points out a sudden decrease of temperature, since a vapour bubble is travelling through it.

The liquid bulk temperature variation along the central axis of the sapphire tube is also calculated during stop-overs and flow oscillations. In microgravity, since the fluid is motionless, heat is exchanged only by conduction, and therefore the liquid slug temperature has no variation along the slug-axis (Fig. 11a). Fig. 11b instead, shows how in hyper-gravity the fluid motion helps the heat transfer as the temperature of the slug decreases going towards the condenser. In this case, the IR analysis can capture a 0.4 K temperature decrease in a 20 mm slug plug.

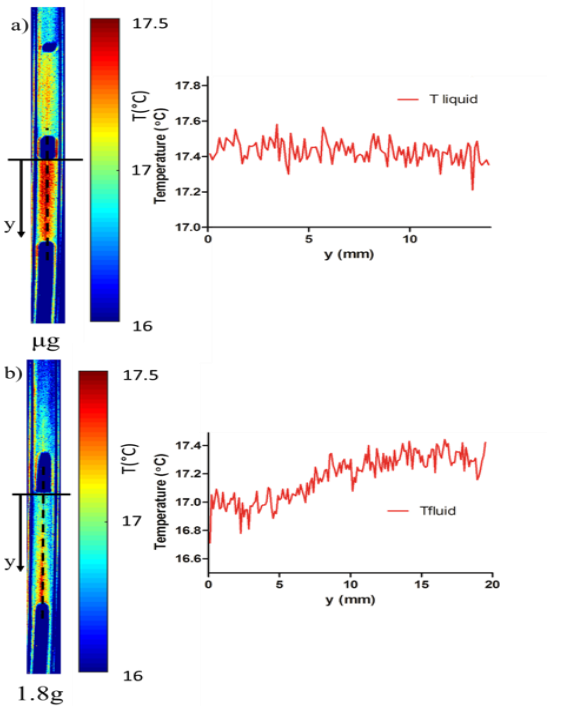

Fig. 11. Liquid bulk temperature calculation in separate instant: a) microgravity and b) hyper-gravity.

5. CONCLUSIONS

A direct IR investigation technique has been adopted to analyse the thermofluidic characteristics of a SLPHP. The ESA MWIR camera has been mounted on a dedicated test-rig for Parabolic Flights (68th ESA PFC) and IR imaging of the fluid with varying gravity field has been obtained. The influence of the condenser temperature on the thermal performances of the SLPHP has been investigated as well. The main outcomes are the following:

- The IR analysis has proven to be a reliable tool in facilitating the recognition of the liquid film dynamics, also indicating wetting/de-wetting phenomena on the inner wall of the sapphire tube with changing gravity field and providing a measure of the liquid temperature increase.
- The IR allows to calculate the liquid slug temperature, with a global accuracy of 1.5 K.
- The synchronization between the time-space maps obtained post-processing the IR images, the velocity of the flow, the pressure measurements at the edges of the sapphire insert and the external wall tube temperature provide an insight of the thermo-fluid dynamics of the two-phase flow in such a PHP section at different g-levels.
- The condenser temperature has a significant effect on the thermo-fluidic behaviour of the device. The data obtained varying the condenser temperature in microgravity on the SLPHP device point out that such a parameter should be carefully considered during the PHP design, especially for space applications.

ACKNOWLEDGEMENTS

The Authors would like to acknowledge UK's EPSRC support through the grant EP/P013112/1 as well as the ESA MAP Project INWIP. The authors would also like to acknowledge the contribution of ESA and NOVESPACE for the opportunity of performing the tests during the 68th PFC. Furthermore, the team would like to thank the TRP project, and the laboratory TEC-MMG at ESA/ESTEC for lending the MWIR camera.

NOMENCLATURE

y	*axial direction of the sapphire tube*
T	*Temperature*
g	*gravity*
min	*minutes*
s	*seconds*
TC	*Thermocouple*
kPa	*kPascal*
α	*Void Fraction*
V_{avg}	*Average Slug Plug Velocity*
L,C,R	*Left, Central and Right Heater*

REFERENCES

1. Akachi H. Structure of a micro-heat pipe, United States Patent, US005219020A. (1993).
2. Marengo M., Nikolayev V.S., Pulsating heat pipes: experimental analysis, design and applications. In: Thome JR, ed. *Encyclopedia of Two-Phase Heat Transfer and Flow IV*. World Scientific, (2018).
3. Zhang Y., Faghri A., Advances and Unsolved Issues

in Pulsating Heat Pipes. *Heat Transfer Engineering* 29 (1) (2008) 20-44.
4. Srinivasan V., Rao M., Khandekar S., Lefèvre F., Bonjour J., Thermo-hydrodynamics of phase-change induced oscillating Taylor bubble flows. *Joint 18th IHPC and 12th IHPS*, Jeju, South Korea (2016) 471–478.
5. Gu J., Kawaji M., Futamata R., Microgravity performance of micro pulsating heat pipes. *Microgravity - Science and Technology* 16 (2005) 181-185.
6. Mameli M., Araneo L., Filippeschi S., Marelli L., Testa R., Marengo M., Thermal response of a closed loop pulsating heat pipe under a varying gravity force. *International Journal of Thermal Sciences* 80 (1) (2014) 11–22.
7. Rao M., Thermo-hydrodynamics of an extended meniscus as unit-cell approach of pul- sating heat pipe. Thermics, INSA de Lyon, (2015).
8. Brusly Solomon A., Karthikeyan V.K., Ramachandran K., Pillai B.C., Effect of number of turns on the temperature pulsations and corresponding thermal performance of pulsating heat pipe. *Journal of Enhanced Heat Transfer* 20 (5) (2013) 443–452.
9. Nekrashevych I., Nikolayev V.S., Effect of tube heat conduction on the pulsating heat pipe start-up. *Applied Thermal Engineering* 11 (2017) 24–29.
10. Manzoni M., Mameli M., de Falco C., Araneo L., Filippeschi S., Marengo M., Advanced numerical method for a thermally induced slug flow: Application to a capillary closed loop pulsating heat pipe. *International Journal for Numerical Methods in Fluids* 82 (7) (2016) 375–397.
11. E J, Zhao X., Deng Y., Zhu H., Pressure distribution and flow characteristics of closed oscillating heat pipe during the starting process at different vacuum degrees. *Applied Thermal Engineering* 93 (2016) 166–173.
12. Pouryoussefi S.M., Zhang Y., Numerical investigation of chaotic flow in a 2D closed-loop pulsating heat pipe. *Applied Thermal Engineering* 98 (2016) 617–627.
13. Gully P., Bonnet F., Nikolayev V.S., Luchier N., Tran T.Q., Evaluation of the Vapor Thermodynamic State in Php. *17th International Heat Pipe Conference* (2013) 1–6.
14. Scammell A., Kim J., Heat transfer and flow characteristics of rising Taylor bubbles. *International Journal of Heat and Mass Transfer* 89 (2015) 379–389.
15. Srinivasan V., Kumar S., Asfer M., Khandekar S., Oscillation of an isolated liquid plug inside a dry capillary. *Heat and Mass Transfer/Waerme- und Stoffuebertragung* (2017) 1–10.
16. Baldassari C., Marengo M., Flow boiling in microchannels and microgravity. *Progress in Energy and Combustion Science* 39 (1) (2013) 1–36.
17. Ilinca A., Mangini D., Mameli M., Fioriti D., Filippeschi S., Araneo L., Roth N., Marengo M., Fluid-flow pressure measurements and thermo- fluid characterization of a single loop two-phase passive heat transfer device *Journal of Physics: Conf. Series* 923 (2017).
18. Luciani S., Brutin D., Le Niliot C., Boiling heat transfer in a vertical microchannel: local estimation during flow boiling with a non intrusive method. *Multiphase Science and Technology* 21 (4) (2009) 297–328.
19. Hetsroni G., Mosyak A., Pogrebnyak E., Rozenblit R., Infrared temperature measurements in micro-channels and micro-fluid systems. *International Journal of Thermal Sciences* 50 (6) (2011) 853–868.
20. Mehta B., Khandekar S., Infra-red thermography of laminar heat transfer during early thermal development inside a square mini-channel. *Experimental Thermal and Fluid Science* 42 (2012) 219–229.
21. Karthikeyan V.K.K, Khandekar S., Pillai B.C.C., Sharma P.K., Infrared thermography of a pulsating heat pipe: Flow regimes and multiple steady states. *Applied Thermal Engineering* 62 (2) (2014) 470–480.
22. Chauris N., Ayel V., Bertin Y., Romestant C., Evaporation of a liquid film deposited on a capillary heated tube: Experimental analysis by infrared thermography of its thermal footprint. *International Journal of Heat and Mass Transfer* 86 (2015) 492–507.
23. Spinato G., Borhani N., D'Entremont B.P., Thome J.R., Time-strip visualization and thermo-hydrodynamics in a Closed Loop Pulsating Heat Pipe. *Applied Thermal Engineering* 78 (2015) 364–372.
24. Liu T.L., Pan C., Infrared thermography measurement of two-phase boiling flow heat transfer in a microchannel. *Applied Thermal Engineering* 94 (2016) 568–578.
25. Fourgeaud L., Nikolayev V.S., Ercolani E., Duplat J., Gully P. In situ investigation of liquid films in pulsating heat pipe. *Applied Thermal Engineering* 126 (2017) 1023–1028.
26. Henry C.D., Kim J., Chamberlain B., Hartman T.G., Heater size and heater aspect ratio effects on subcooled pool boiling heat transfer in low-g. In: *Experimental Thermal and Fluid Science*, 29 (2005) 773–782.
27. Mameli M., Mangini D., Vanoli G.F.T., Araneo L., Filippeschi S., Marengo M., Advanced multi-evaporator loop thermosyphon. *Energy* 112 (2016) 562–573.
28. Mangini D., Ilinca A.I., Mameli M., Fioriti D., Filippeschi S., Araneo L., Marengo M., Single loop pulsating heat pipe with non-uniform heating patterns: fluid infrared visualization and pressure measurements. *9th World Conference on Experimental Heat Transfer, Fluid Mechanics and Thermodynamics*, Iguazu Falls, Brazil (2017).
29. Sobac B., Brutin D., Thermocapillary instabilities in an evaporating drop deposited onto a heated substrate. *Physics of Fluids*, 24 (3) (2012)
30. Pietrasanta L., Mangini D., Fioriti D., Miche N., Andredaki M., Georgoulas A., Araneo L., Marengo M., A single Loop pulsating heat pipe in varying gravity conditions: experimental results and numerical simulations. *Proc. 16th Int. Heat Transf. Conf. IHTC-16 August 10-15*, Beijing, China Full Paper accepted *(*2018).
31. Catarsi A, Fioriti D, Mameli M, Filippeschi S, Di Marco P. Accuracy analysis of direct infrared temperature measurements of two-phase confined flows,*Proceedings of the 16th International Heat Transfer Conference, IHTC-16 August 10-15, 2018, Beijing, China Full paper accepted*; (2018).